InterPore JOURNAL

Original Research

ON THE INTERPRETATION OF UNSTEADY STATE EXPERIMENTS IN HETEROGENEOUS ROCK BY STOCHASTIC METHODS

Omidreza Amrollahinasab, Boris Jammernegg, Siroos Azizmohammadi, Holger Ott

Department Geoenergy, Montanuniversität Leoben, Leoben, Austria

Correspondence to:
Holger Ott,
holger.ott@unileoben.ac.at

How to Cite:
Amrollahinasab, O., Jammernegg, B., Azizmohammadi, S., & Ott, H. On the Interpretation of Unsteady State Experiments in Heterogeneous Rock by Stochastic Methods. *InterPore Journal*, *2*(2), IPJ040625–5. https://doi.org/10.69631/ipj.v2i2nr44

RECEIVED: 13 Sept. 2024
ACCEPTED: 6 Apr. 2025
PUBLISHED: 4 Jun. 2025

ABSTRACT

Rock heterogeneity has a significant effect on immiscible displacement. This is especially true when the mobility ratio of the two fluids is unfavorable, favoring unstable displacement. However, this is not taken into account in the numerical analysis of classical core flooding experiments to quantify two-phase flow properties using Special Core Analysis (SCAL). Our approach combines the modern interpretation of SCAL data with experimental data measured on rock samples for which the homogeneity assumption—a prerequisite for SCAL experiments—can no longer apply due to their size and heterogeneity. In contrast to other studies that take heterogeneities into account, we focus on simple-to-perform unsteady-state experiments. We analyze these experiments by numerical interpretation using homogeneous and heterogeneous simulation domains and by introducing porosity-based heterogeneity and permeability as well as capillary scaling. In the current study, we first question the applicability of standard relative permeability measurements to heterogeneous rocks and fluids with an excessively high mobility ratio, such as for CO_2-brine displacement in heterogeneous rocks. However, we show that they describe two-phase flow very well when porosity-based heterogeneity is taken into account, which is equivalent to downscaling. The study thus shows a way to fall back on established standard measurements if it should be possible to account for subgrid heterogeneities in SCAL workflows. To this end, we propose an approach based on steady-state experiments and appropriate sample selection.

KEYWORDS

Special core analysis, CO_2 sequestration, Unsteady-state experiments, Relative pereability, Capillary heterogeneity, Upscaling

1. INTRODUCTION

Among the many applications that require accurate predictions of two-phase fluid displacements are hydrocarbon recovery and geologic CO_2 storage. However, the unexpected migration of carbon dioxide during CO_2 injection highlights the need to better understand the underlying mechanisms, especially in heterogeneous reservoirs (2, 15, 29, 33). It is well known that rock formations are heterogeneous at various scales. However, experiments to measure flow properties require samples in which the rock properties are well represented and are not dependent on the specific sample volume, i.e., a volume larger than the representative elementary volume (REV) (4). As a result, the design and interpretation of multiphase flow property measurements is challenging because the definition of an REV depends on both the scales of heterogeneity and the nature of the property being measured (13, 16, 45, 50). Due to the dependence of capillary forces on heterogeneity, local variations in saturation states during immiscible displacements are known as 'capillary heterogeneity'. This effect can be conceptualized in terms of the spatial variability of capillary pressure saturation functions (11). This phenomenon has practical implications since the measurement of multiphase flow parameters is affected by the scale of investigation (17, 23, 44). Submeter-scale rock heterogeneity, such as laminations and bedding, can significantly affect fluid flow properties and should be considered when modeling or predicting fluid flow at larger scales (5, 17, 49). This effect is particularly pronounced in multi-scale heterogeneous carbonates and for strong fluid-viscosity contrasts, such as CO_2-brine displacement.

In conventional reservoir simulation workflows, small-scale heterogeneity is not explicitly captured due to the typically large grid block sizes to which multiphase flow properties are assigned (12, 18, 42). A key input function in immiscible displacement is the relative permeability, which controls displacement and sweep efficiency. Typically, laboratory and special core analysis (SCAL) measurements are performed on homogeneous samples that do not accurately represent the average property at the discretization size of a reservoir model. This poses a significant challenge to the characterization or measurement of relative permeability. To illustrate this point, we can compare the size of a SCAL plug, which is in the order of centimeters, to a typical grid block in a reservoir simulation, which can be orders of magnitude larger. Our understanding of the process of upscaling homogeneous rock/fluid properties (SCAL) to the next larger scale is limited because of the typically limited information available from the subsurface about mesoscale heterogeneity, but also because of our inability to describe rock heterogeneity well enough. Several approaches have been developed to characterize capillary heterogeneity in rock cores (5, 19, 20, 21, 22, 24, 32, 38, 39, 43). However, uncertainties remain in the characterization and description of more complex rocks, especially for multiphase flow along fractional flow curves and for different flow rates (6, 7).

There are workflows from the pore scale to the meter scale that provide new opportunities to systematically upscale multiphase flow for reservoir applications (25). These workflows combine laboratory measurements, such as core flooding, with in situ imaging methods at various scales and digital rock physics with upscaling schemes that incorporate capillary pressure heterogeneity into the analysis. With rigorous upscaling, small-scale effects can be incorporated into continuum-scale models by interpreting them through numerical modeling using an optimization routine; effective petrophysical parameters and relative permeability saturation functions are calculated, and their uncertainties are included (3, 10, 16, 25, 38, 46). In practice, however, the implementation of sample heterogeneity for relative permeability interpretation refers to downscaling rather than upscaling, unless the heterogeneity is represented in a reservoir grid block.

In addition to the core-scale workflows mentioned above, there is a well-established body of work on deriving relative permeability and capillary pressure directly from pore-scale simulations. Pore-network models, for instance, describe the pore space as interconnected pores and throats, making it possible to simulate multiphase flow under various wettability conditions (7, 8, 27, 34, 41, 47). Similarly, lattice Boltzmann methods and similar direct numerical simulations capture interfacial dynamics in micro-CT images of rocks (1). Although these approaches provide valuable insights into pore-scale physics, they often require detailed digital rock imaging and can be computationally demanding. They also raise issues of upscaling, as relative permeability and capillary pressure relationships must be integrated over

potentially complex heterogeneities. The present study therefore focuses on unsteady-state experiments on larger, more heterogeneous rock samples, bridging the gap to scales where heterogeneity plays a dominant role.

The Estaillades limestone is a candidate rock sample with a high degree of heterogeneity. It has been shown that traditionally measured relative permeability saturation functions are insufficient to represent a rock volume that is an order of magnitude larger (37). In a follow-up investigation, we developed a rigorous and fully stochastic SCAL analysis workflow and applied it to steady-state and centrifuge experimental data on decane-brine primary drainage in Estaillades. The analysis provided confidence intervals for the combined measurements and sample-to-sample variation (3). The present study compares these results to larger scale unsteady state (USS) core flooding experiments using 1D homogeneous simulation domains. By assuming homogeneity, which is traditionally the case for SCAL data interpretation (31), the analysis of the USS experiment directly provides the upscaled $k_r(S_w)$, including the confidence interval, which is representative for the specific sample size. In a second step, we implement the X-ray computed tomography (CT) porosity profile and the resulting capillary heterogeneity and permeability profiles. By history matching the USS experiment to the 3D heterogeneous domain, we can determine the true $k_r(S_w)$ and the effects of heterogeneity on the scales studied.

Using decane-brine and CO_2-brine transient experiments, we investigate the effect of heterogeneity on the relative permeability. Using the water-wet reference case, previous steady-state measurements are directly compared to the system under study. In this step-by-step approach, heterogeneity is introduced by first considering a 1D homogeneous simulation domain, then a 1D heterogeneous simulation domain, and finally a 3D heterogeneous domain. As a result, we perform a full stochastic analysis for homogeneous 1D cases. Using simple history matching, we derive the base case $k_r(S_w)$ for the 1D heterogeneous domain, which is also used for 3D simulations. As the fluid pairs and simulation domains become more complex, we ensure that the method is robust and able to handle a wider range of heterogeneities. Using this methodology, we can gain valuable insights into the validity and limitations of the current SCAL procedures and develop alternative methods and upscaling workflows for the calculation of saturation functions. The developed numerical workflow can be extended to other highly heterogeneous and demanding rock-fluid systems.

2. EXPERIMENTAL AND NUMERICAL METHODS

In this work, the experimental results are based on those published in Ott et al (37). The experiments were performed on Estaillades limestone samples with a length of 15 cm and a diameter of 7.5 cm. The average porosity and the average permeability of the rock sample were measured to be $\phi = 0.297$ and $K = 260$ mD, respectively.

The experiments were performed at a pressure of 100 bar and a temperature of 50°C, which corresponds to a reservoir depth of about 1000 m at which the injected CO_2 is in a supercritical (sc) state. At this thermodynamic condition, the CO_2, decane, and brine phases have densities of $\rho_{CO2} = 384.67$ kg/m^3, $\rho_{decane} = 707.3$ kg/m^3, and $\rho_{brine} = 1001.2$ kg/m^3, and viscosities of $\mu_{CO2} = 0.0309$ cP, $\mu_{decane} = 0.619$ cP, and $\mu_{brine} = 0.576$ cP, respectively. To investigate the primary displacement process of brine by CO_2, a sample was first saturated to $S_w = 1$ and then flooded with scCO_2. A reference measurement was performed on the same sample using decane as the injection phase. Since the SCAL measurements (37) were performed with the same fluid pair and on the same rock type from the same block of the Estaillades outcrop, the decane-brine experiments serve as a reference and are directly comparable to the previous SCAL interpretation (3). The flooding experiments were conducted in USS using constant injection rates of 0.25 ml/min for decane injection and 0.44 ml/min for CO_2 injection. These flow rates correspond to a capillary number of $Ca \sim 5 \times 10^{-8}$ for decane-brine and $Ca \sim 6 \times 10^{-9}$ for CO_2-brine. During the experiments, the pressure drop was measured, and the up-front 3D porosity profiles as well as the 3D saturation profiles were obtained using differential imaging conducted during medical CT scanning. Production curves were determined by monitoring CT saturation. In **Figure 1**, the saturation

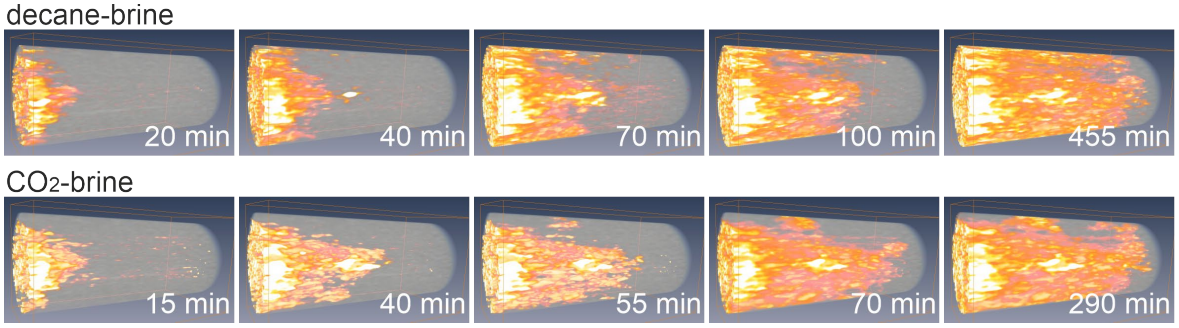

Figure 1: Computed tomography images taken during decane-brine (top) and CO_2-brine (bottom) primary drainage experiments. Both experiments were performed in sequence on the same rock sample. The data were recorded in differential imaging to highlight the saturation distributions for the invading decan and CO_2. The initial rock-fluid system is shown as a semitransparent background. Note that the saturation thresholds are comparable but arbitrarily chosen to highlight the heterogeneity in the saturation distributions. The absolute saturation values are shown in **Figure 2 c,f** and **Figure 4 c,f** for 1D saturation profiles and in **Figure 6 a,e** for 3D volumes.

profiles for the displacements of decane-brine (top row) and CO_2-brine (bottom row) are shown in orange and the initial rock-fluid system is semitransparent in the background. Both experiments were performed in a sequence on the same rock sample. The experimental details can be found in Ott et al (37).

The simulations performed in this study use the MATLAB Reservoir Simulation Toolbox (MRST). The experiments are simulated as displacement of immiscible, incompressible fluids, and consequently the material balance for incompressible two-phase flow and two-phase Darcy's equation (momentum balance) are solved. The input parameters are the measured sample porosity and permeability, the CT-based 1D and 3D porosity profiles, and the fluid phase densities and viscosities as given above. The simulation results are then subjected to history matching, which matches and optimizes the simulation results to the experimental measurements. MATLAB's global optimization module was used to accomplish this task. Based on genetic or active-set algorithms, this module performs a constrained nonlinear optimization to introduce essential inequalities consistent with the saturation function parameters in the study. After achieving the best fit, we examine the response surface around the optimal solution and determine the sensitivity of the optimal solution using Markov Chain Monte Carlo (MCMC), specifically the Delayed-Rejection Adaptive-Metropolis (DRAM) algorithm. As a result of the DRAM approach, the MCMC sampler becomes more efficient and can handle high-dimensional problems resulting from the large number of parameters inherent in saturation functions. An optimal solution to the complex task of history matching and uncertainty analysis is provided by the combination of numerical techniques and simulation methods. Amrollahinasab et al (3) discusses the methodology and how it is applied to transient experiments in the current study. The analysis and numerical treatment of the rock heterogeneity is part of the results and is embedded in the following chapter.

3. EXPERIMENTAL AND NUMERICAL METHODS

3.1. Data Interpretation Assuming Homogeneity

In the classical SCAL interpretation, it is assumed that the samples are homogeneous and can be described with a homogeneous 1D simulation domain. To fulfill this assumption, the samples must be carefully selected and must correspond to a representative elementary volume (REV). As a result, the samples are quite small with diameters of 1 or 1.5 inches and a length of a few centimeters. The evaluation of the experimental data usually provides a single set of relative permeability $k_r(S_w)$ and capillary pressure $P_c(S_w)$ saturation functions, which in themselves require no further interpretation. In reservoir simulations, these saturation functions are then assigned to rock types, with heterogeneity accounted for by a Leverett-J scaling of $P_c(S_w)$ (26). An individual grid block is then assigned to a single

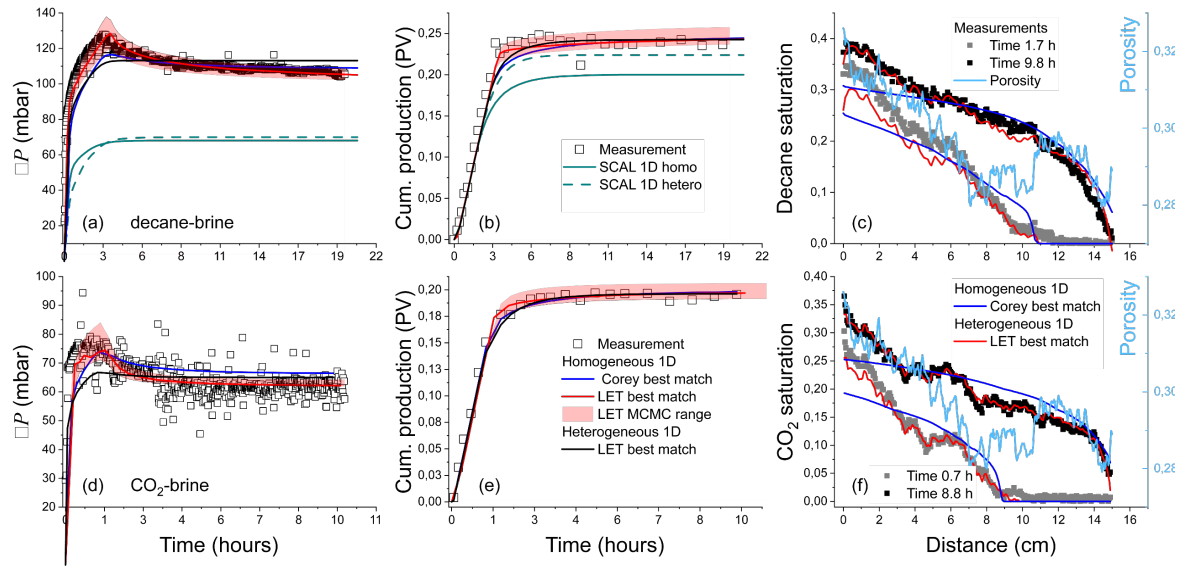

Figure 2: The experimental responses (symbols) of the decane-brine (top row) and CO_2-brine (bottom row) displacement experiments in **Figure 1** and their numerical interpretation. From left to right: Pressure difference and brine production curve as a function of time, and the decane and CO_2 saturation profiles at two consecutive time steps, as indicated in the legend. The lines correspond to forward simulations using SCAL data (petrol, SCAL 1D homo/hetero) and to numerical 1D history-matching results using 1D homogeneous and heterogeneous simulation domains (blue, Corey and red, LET (28)) computed from the CT density profile (light blue). Detailed descriptions of the relative permeability representations and uncertainty intervals are given in the text and in the legend.

set of $k_r(S_w)$ and $P_c(S_w)$ saturation functions, meaning that the grid block is described as homogeneous in all respects.

In contrast to small-scale SCAL experiments, core flooding at larger scales is typically influenced by sample size and heterogeneity, leading to sweep effects (5, 37). To interpret the data numerically, there are two possibilities: **a)** including rock heterogeneity explicitly in the simulation model to obtain "true" saturation functions, which effectively refers to a down-scaling, and **b)** ignoring rock heterogeneity, i.e. assuming a homogeneous and representative rock volume. We can assume that in the latter case we will not find the same relative permeability as for case (a), but an effective $k_r(S_w)$ that is representative of the investigated volume. We refer to this as the upscaled $k_r(S_w)$, which may still be scale dependent.

Using a 1D homogeneous simulation domain (case (b)), we first derive the relative permeability from the larger scale USS experiments. Using the SCAL-derived $k_r(S_w)$ and $P_c(S_w)$ (3), we first forward-simulate the displacement to check the validity of the SCAL input. In a second step we try to match the experimental data to determine $k_r(S_w)$ using MICP-derived $P_c(S_w)$, data typically available from routine core analysis. The MICP curve is scaled according to the interfacial tension (IFT) for the primary drainage (**Eq. 1**):

$$P_c(\sigma) = \frac{\sigma \cos\theta}{\sigma_{ref} \cos\theta_{ref}} \, p_{c,ref}, \tag{1}$$

where σ_{ref} is the mercury-air IFT (480 mN/m), θ_{ref} is the corresponding contact angle, which is assumed to be the same for both non-wetting fluids ($\theta_{ref} = \theta$). σ is the IFT of the decane- or CO_2-brine systems, which are assigned 45 mN/m and 40 mN/m, respectively (14). The closure correction is also applied to the MICP using the methodology presented in McPhee et al (31). The pressure drop and data were then fitted by varying $k_r(S_w)$. The comparison of the MICP-scaled decane-brine $P_c(S_w)$ with that derived from SCAL measurements, including the uncertainty range, is reported in a previous study (3)

and is shown in **Figure 3 c,f** for decane-brine and CO_2-brine; the scaled MICP curve is well within the uncertainty range of the SCAL data, except for the inlet pressure.

Due to the common rock-fluid system (decane-brine), the SCAL-interpreted $k_r(S_w)$ and $P_c(S_w)$ from our previous study (3) can now be directly compared with the decane-brine USS flooding experiment. Forward simulations of the USS process using the SCAL-derived saturation functions showed large deviation between the predicted and experimentally observed results; the pressure drop and the brine production curve are strongly underestimated, as shown in **Figure 2 a,b** – the SCAL data obtained from small samples are not directly applicable, not even to the next larger scale investigated.

A good match is achieved by history matching the experimental data using the two commonly used parameterizations of $k_r(S_w)$, Corey (9) and LET (28). The Corey parameterization was used and the residual decane saturation and the corresponding endpoints were fixed at $S_w = 1$ and $k_r(S_w = 1) = 1$, corresponding to a primary drainage process, but all other parameters were free and could be matched. **Figure 2** shows the matched experimental pressure drop, production curve, and saturation profiles. The results show that the cumulative brine production and the pressure difference generally agree well, with some deviations in the transient part and especially at the breakthrough point, although the saturation profiles simulated on a homogeneous domain cannot reflect the experimental profiles in most cases.

An alternative method for matching experimental measurements using 1D homogeneous models is the LET parameterization, which offers more flexibility but also requires more fitting parameters. Markov Chain Monte Carlo simulations were used for the uncertainty analysis, similar to the SCAL results (3). It is important to note that in the present case, $P_c(S_w)$ remains constant with respect to the scaled MICP discussed earlier.

Figure 3 a,b show the history match results and quantified uncertainty ranges along with the best fits from the SCAL interpretation. Even if the experimental responses are perfectly described with the LET model, the relative permeability curves deviate significantly with the state-of-the-art SCAL $k_r(S_w)$. On a larger scale, the fluid phases show significantly lower mobility and are in fact well outside the confidence

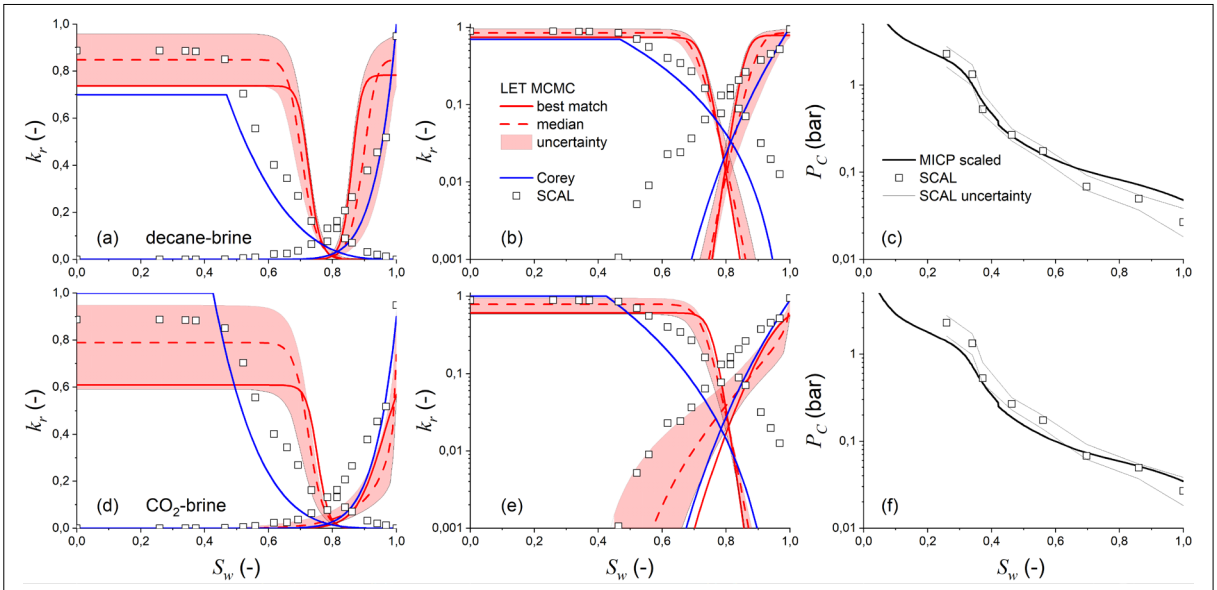

Figure 3: Relative permeability saturation functions resulting from history matching on 1D homogeneous and 1D heterogeneous simulation domains. The capillary pressure functions on the right are used as input (see text). The top row panels (a) to (c) show the HM results of the decane-brine, and the bottom row panels (d) to (f) show the results of the CO_2-brine displacement experiments. From left to right: $\boldsymbol{k_r}$ on a linear and logarithmic scale, and $\boldsymbol{P_c}$ on a logarithmic scale. The squares correspond to the SCAL results measured on a smaller scale and considered homogeneous.

 https://doi.org/10.69631/ipj.v2i2nr44

intervals given for both the SCAL data (3) and the USS LET data. As expected, the simulated saturation profiles in **Figure 2** show poor agreement with the experimental; in particular, a homogeneous simulation domain cannot represent a saturation state in heterogeneous rock sample, but the overall material balance as represented by the brine production curve is accurate.

The same procedure was applied to the CO_2-brine displacement experiment, with the results shown in the bottom row of **Figure 2**. A similar picture can be drawn as that for the decane-brine experiment. A history fit using homogeneous rock properties, a LET representation of $k_r(S_w)$ and the MICP derived $P_c(S_w)$ shows a good fit to the experimental responses in **Figure 2 d,e**; the MCMC confidence interval (P10 to P90) covers the experimental data points well. **Figure 2f** shows the saturation profiles for two consecutive time steps. Again, the complexity of the experimental saturation profile cannot be matched, but the material balance can be. The resulting $k_r(S_w)$ values are shown in **Figure 3 d,e**. A similar tendency is observed for the CO_2-brine system as for the decane-brine system discussed above, with $k_r(S_w)$ showing a distinctly different behavior than that derived by SCAL.

Using a 1D homogeneous model match data from homogeneous rock samples, we conclude the following: **a)** History matching complex experimental data with assumed homogeneous rock properties allows an accurate description of the experimental ΔP and the brine production curve. **b)** Due to the homogeneity assumption, the simulated saturation profiles $S_w(x)$ cannot match the complex experimental profiles, but are in agreement with the material balance. **c)** For the investigated sample volume, $k_r(S_w)$ can therefore be considered as upscaled and representative by the homogeneity assumption, however it differs significantly from the SCAL-derived $k_r(S_w)$ and may still be scale-dependent.

3.2. Introducing Heterogeneity

To capture the diverse saturation profiles shown in **Figure 2 c,f**, we use the approach developed by Hosseinzadeh Hejazi et al (16). In this method, core heterogeneity is addressed by adjusting the capillary pressure within each grid block. Our implementation divides the 1D simulation domain into 2 mm slices, which allows for a detailed representation of the sample heterogeneity. Each slice, denoted as j, is uniquely defined by its capillary pressure $P_c^j(S)$, porosity ϕ_j, and absolute permeability K_j. This method allows for the evaluation of small-scale fluid saturation variations due to capillary heterogeneity by analyzing changes in the capillary entry pressure of each grid (16). According to the Brooks-Corey model (9), the entry pressure, P_d, is a critical parameter, leading to the scaling relation (**Eq. 2**):

$$P_c^j(S) = \frac{1}{f_j} P_c(S) = \frac{P_{dj}}{P_d} P_c(S) \qquad j = 1, \dots, N, \tag{2}$$

where f_j is the scaling factor for each grid j, N is the total number of elements, and P_{dj} is the entry pressure for the jth element. The reference capillary pressure curve, $P_c(S)$, is determined by SCAL experiments. Using Brooks-Corey parameters for this reference curve allows one to accurately model system capillary pressures. Porosity and permeability spatial variations are evaluated using the Leverett-J function, $J(S)$, which is defined as (**Eq. 3**):

$$J(S) = \sqrt{\frac{K}{\phi}} \frac{P_c(S)}{\gamma}. \tag{3}$$

This is used to formulate the scaling factor, which corresponds to a Leverett-J scaling (**Eq. 4**):

$$f_j = \frac{P_d}{P_{dj}} = \sqrt{\frac{K_j/\phi_j}{K_\mathrm{m}/\phi_\mathrm{m}}}, \tag{4}$$

where K_j and ϕ_j are the permeability and porosity for each grid, and K_m and ϕ_m are the respective measured average values. For heterogeneous models, the saturation profile is then derived close to steady state from (**Eq. 5**):

$$\frac{\mathrm{d}S}{\mathrm{d}x_{\mathrm{D}}} = \left(\frac{q\mu_{\mathrm{nw}}I}{AK_j}\right)\left(\frac{1}{k_{\mathrm{r,nw}}(S)}\right)\left(\frac{f_j}{\mathrm{d}P_{\mathrm{c}}(S)/\mathrm{d}S}\right). \tag{5}$$

To analyze the individual elements, the saturation and capillary pressure of each grid cell are adjusted by the scaling factor f_j in our MRST-based simulator. To determine the optimal values for these scaling factors, we use an objective function that aims to minimize the discrepancy between the experimental and simulated capillary pressure profiles. This objective function is given by (**Eq. 6**):

$$E(x_j) = \sum_{k=1}^{N_{\mathrm{q}}} \left(\frac{P_{\mathrm{c}}\left(S^{\mathrm{exp}}(x_j)\right) - f_j P_{\mathrm{c}}\left(S^{\mathrm{H}}(x_j)\right)}{P_{\mathrm{c}}\left(S^{\mathrm{exp}}(x_j)\right)}\right)^2, j = 1, \ldots, N, \tag{6}$$

where P_{c} is the reference capillary pressure curve, f_j is the scaling factor, $S^{\mathrm{exp}}(x_j)$ is the slice-averaged experimental water saturation and $S^{\mathrm{H}}(x_j)$ is the saturation profile derived from homogeneous simulations. This methodology accounts for the fact that capillary pressure reference curve is largely unaffected by small-scale heterogeneities and thus justifies our approach (16).

After determining the scaling factors using **Equation 6**, we proceed to calculate the properties of the heterogeneous model. In particular, we calculate the K_{hm} using **Equation 4** and the porosity profile shown in **Figure 2 c**. For the purpose of heterogeneous modeling, each grid cell is characterized by three different properties: the porosity ϕ, the absolute permeability K calculated from **Equation 4**, and the capillary scaling factor f derived from **Equation 6**.

To validate our model, we perform a comparison of numerical responses such as pressure difference (ΔP), brine production (Q), and saturation profiles ($S(x)$) with experimental measurements. This process involves a multiobjective optimization approach that uses a genetic algorithm from the MATLAB optimization toolbox to minimize a three-part composite error function (**Eq. 7**)

$$\begin{aligned} I &= \frac{1}{N}\sum_{j=1}^{N}\left(\frac{\Delta P^{\mathrm{sim}}(x_j) - \Delta P^{\mathrm{exp}}(x_j)}{\Delta P^{\mathrm{exp}}(x_j)}\right)^2, \\ J &= \frac{1}{N}\sum_{j=1}^{N}\left(\frac{Q^{\mathrm{sim}}(x_j) - Q^{\mathrm{exp}}(x_j)}{Q^{\mathrm{exp}}(x_j)}\right)^2, \\ K &= \frac{1}{N}\sum_{j=1}^{N}\left(\frac{S^{\mathrm{sim}}(x_j) - S^{\mathrm{exp}}(x_j)}{S^{\mathrm{exp}}(x_j)}\right)^2. \end{aligned} \tag{7}$$

This rigorous approach allows us to fine-tune our model to ensure that it accurately reflects the experimental data, thereby confirming its accuracy. In addition, the methodology incorporates a new perspective by analyzing scaling factors derived from single-rate drainage experiments. This includes the evaluation of saturation profiles under both transient and steady-state conditions towards the end of the injection period. Such analysis enriches our understanding by incorporating dynamic saturation changes into the modeling process and provides a more comprehensive view of fluid behavior in the reservoir.

3.3. Data Interpretation Considering the 1D Porosity Profile

In the next step, we include porosity, permeability, and capillary heterogeneity according to the above model in a 1D simulation domain. The inclusion of heterogeneity based on the exact porosity profile allows a more complete description of the experimental data with minimal additional parameters, such as the scaling factor. The agreement obtained with the experimental responses is shown in **Figure 4** for both systems, decane-brine and CO_2-brine. While the saturation profiles and brine production curves are accurately described, discrepancies in the differential pressure ΔP are observed in the transient behavior around the breakthrough time.

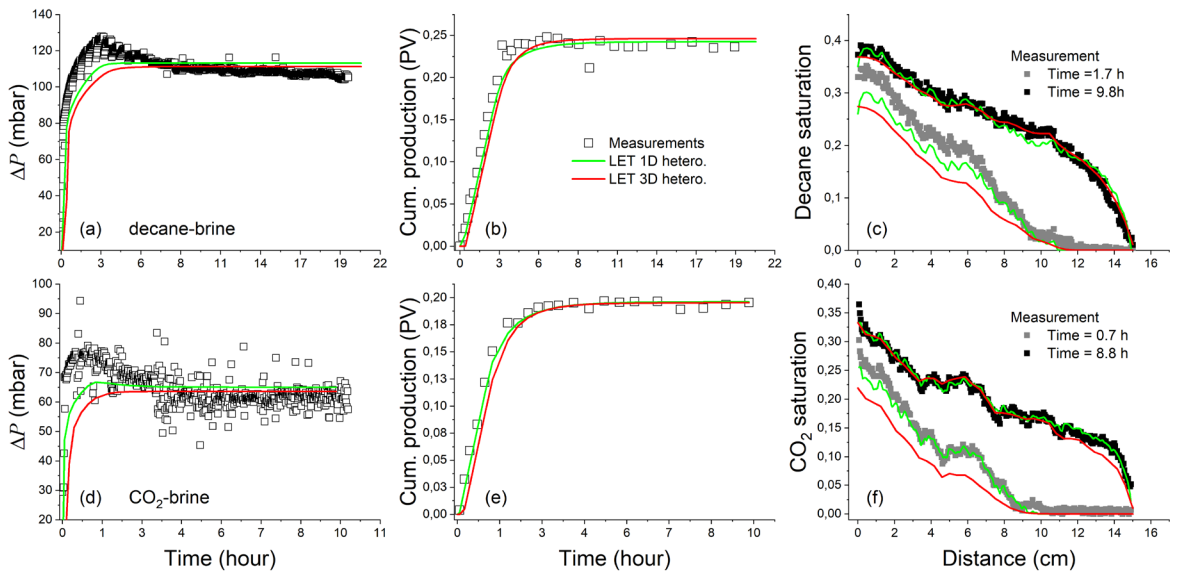

Figure 4: The experimental responses (symbols) of the decane-brine (top row) and CO_2-brine (bottom row) displacement experiments and their numerical interpretation as in **Figure 2**. From left to right: Pressure difference and brine production curves as a function of time, and the decane, CO_2 saturation profiles at two consecutive time steps, as indicated in the legend. The lines correspond to the numerical history matching results using a 1D heterogeneous domain computed from the CT density profile and the full 3D heterogeneous volume. The relative permeability representations used are indicated in the legend and described in the text.

Figure 5 shows the Corey and LET $k_r(S_w)$ and Brooks-Corey $P_c(S_w)$ together with the SCAL interpretations, and illustrates that the inclusion of heterogeneity in the simulations significantly reduces the gap between the model predictions and the uncertainty range of the SCAL interpretation. In particular, the decane $k_r(S_w)$ is well described on both the linear and logarithmic scales, and the brine $k_r(S_w)$ is well described on the linear scale, i.e. for large water mobility. It should be noted that the uncertainty range from our previous work (3) describes the uncertainty of the measurement, but not the sample-to-sample variation, i.e. the heterogeneity. The good agreement of the simulation with the experimental data therefore shows that conventionally measured relative permeabilities describe heterogeneous systems well, provided that heterogeneity has been explicitly introduced into the model calculation as described above. It is also noteworthy that the decane $k_r(S_w)$ falls well within this uncertainty interval, while the CO_2 $k_r(S_w)$ deviates significantly from the SCAL predictions. This difference is probably due to different wetting properties in the decane-brine system compared to the CO_2-brine system.

The study highlights the importance of interpreting measurement data in the context of the phenomena under investigation and confirms the effectiveness of the methodology developed for steady-state experiments by Hosseinzadeh Hejazi et al (16) for USS drainage experiments. Moreover, the analysis of the scaling factors and Pareto fronts resulting from the optimization method used shows a linear relationship between production errors and errors in the saturation profile. This observation corrects the

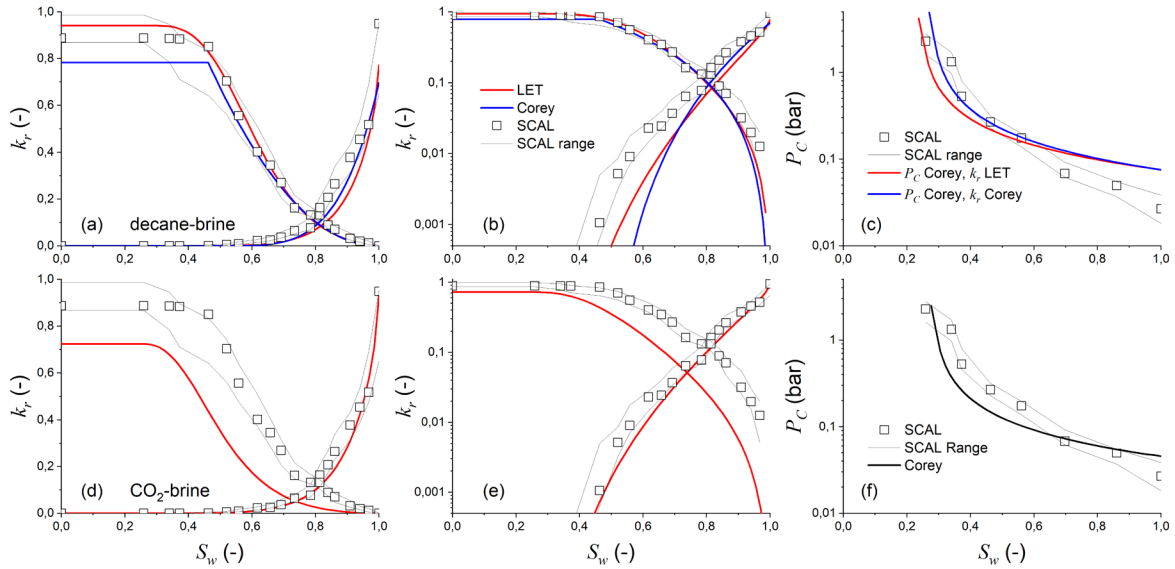

Figure 5: Relative permeability and capillary pressure saturation functions resulting from experiments and history matching on the 1D and 3D heterogeneous simulation domains. The top row (a, b, c) shows the HM results for the decane-brine experiments, and the bottom row (d, e, f) shows the results of the CO_2-brine displacement experiments. From left to right: $\boldsymbol{k_r}$ on a linear and a logarithmic scale, and $\boldsymbol{P_c}$ on a logarithmic scale. The squares correspond to the SCAL results measured on a smaller scale, and are considered homogeneous.

inconsistencies found in homogeneous simulations and highlights the need for heterogeneity in simulations to achieve a more accurate and comprehensive understanding of the system under study.

3.4. Modeling the 3D Heterogeneous Volume

3.4.1. Transforming Medical CT Data into 3D Porosity and Saturation Maps

This section explains the process of converting medical CT scans into 3D porosity and fluid-saturation maps. The individual scans are represented on a gray scale in Hounsfield Units (HU), an absolute scale for medical applications. Prior to further processing, the scans were subjected to median filtering and 3D Gaussian blurring to reduce noise and better determine the porosity profile and saturation state.

The 3D porosity map was obtained using differential imaging. This approach calculates the difference between brine saturated and dry scans as recommended by various studies (35, 36, 48). The voxel-by-voxel porosity profile is derived using **Equation 8**:

$$\phi(\vec{x}) = \frac{HU^{sat}_{brine}(\vec{x}) - HU_{dry}(\vec{x})}{HU_{brine} - HU_{air}} = \alpha \cdot \left(HU^{sat}_{brine}(\vec{x}) - HU_{dry}(\vec{x})\right), \tag{8}$$

where $HU^{sat}_{brine}(\vec{x})$ is the HU value for the voxel in the brine-saturated scan, $HU_{dry}(\vec{x})$ is for the dry scan, and HU_{brine} and HU_{air} are the HU values for brine and air, respectively. The difference is then scaled by a factor α to match the measured sample porosity.

Subsequently, the 3D fluid saturation maps were determined for the time lapse CT scans ($HU_{exp}(\vec{x}, t)$) by **Equation 9**:

 https://doi.org/10.69631/ipj.v2i2nr44

$$S_{CO_2}(\vec{x},t) = \frac{HU^{sat}_{brine}(\vec{x},t_0) - HU_{exp}(\vec{x},t)}{HU^{sat}_{brine}(\vec{x}) - HU^{sat}_{CO_2}(\vec{x})}, \quad (9)$$

where $HU^{sat}_{brine}(\vec{x},t_0)$ and $HU^{sat}_{CO_2}(\vec{x})$ correspond to the calibration scans at $S_w = 1$ and $S_w = 0$, respectively, and $HU_{exp}(\vec{x},t)$ are scans at individual time steps. Resulting 3D saturation maps are shown in **Figure 6 a,e**.

The original resolution of these CT images (voxel size) was 0.18×0.18×0.5 mm³. To increase the efficiency of the computations, the data were binned by combining 24×24×8 voxels into blocks of approximately 4 mm³. The impact of this voxel binning on simulation accuracy was evaluated by comparing it to a finer binning of 12×12×4 voxels, specifically for the decane-brine scenario. This comparison showed negligible differences in the results, so that the simulations were carried out on the coarser grid for reasons of computing time.

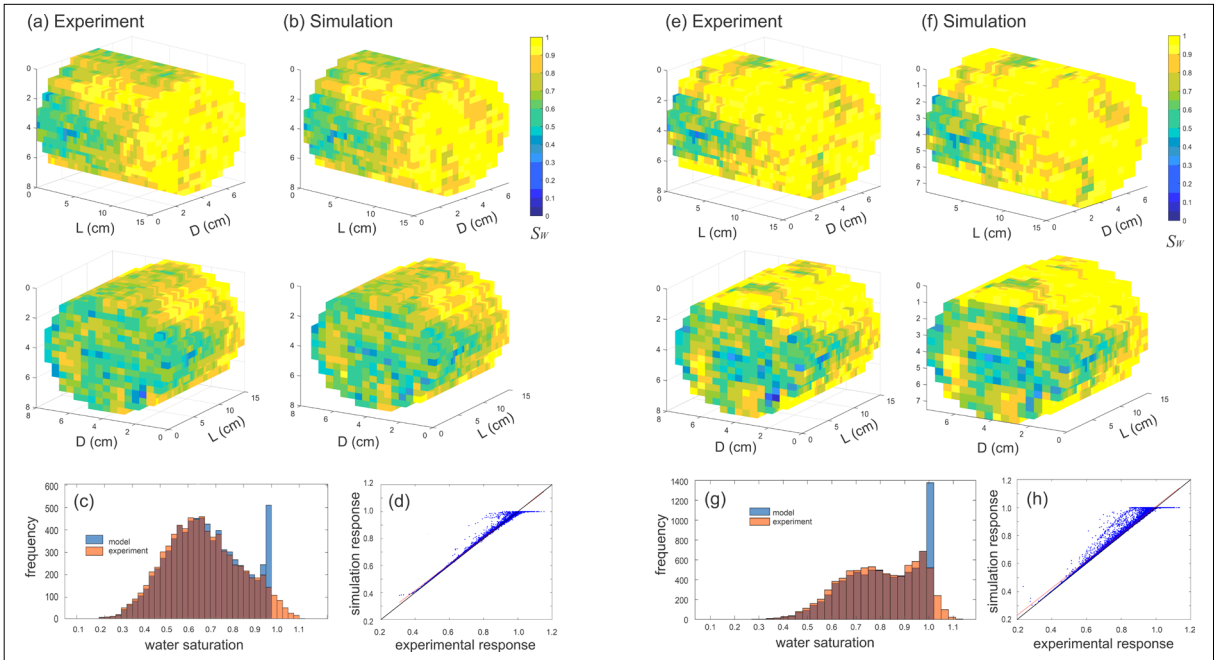

Figure 6: a) Measured 3D water saturation profiles after 9.8 h of decane flooding. Flow direction is from left to right. **b)** Corresponding simulation output. **c)** Comparative experimental and simulated water saturation histograms and **d)** correlation between simulated and experimentally measured saturations. The black line shows the slope of unity with zero intercept. The red line shows a linear regression on the data. Parts **(e)** through **(h)** show the same data after 8.9 h of CO_2 flooding.

3.4.2. 3D Heterogeneous Modeling

The capillary pressure scaling described above was extended to the 3D simulation domain. The same principle used to determine the scaling factors in 1D was applied to the 3D grid. However, instead of attempting to fit the model to the experimental data in 3D, due to the available computational power, the study performed forward simulations using the best fit of the 1D modeling (LET 1D heterogeneous). The agreement between the simulated and experimental fluid saturation distributions was then statistically analyzed for evaluation.

The comparison between observed and predicted saturation values, detailed in **Figure 6** for both decan brine and CO_2-brine displacement, uses 1D saturation profile projections (**Fig. 4**) in addition to the experimental data to provide a more effective assessment. Despite the simple forward simulation, the agreement between 3D simulations, 1D projections and experimental data is found to be satisfactory. The study shows that both the differential pressure (ΔP) and the cumulative brine production in the 3D

 https://doi.org/10.69631/ipj.v2i2nr44

simulations agree well with those of the heterogeneous 1D modeling, although with similar limitations in terms of the data on the respective breakthrough times. This limitation suggests potential challenges associated with the capillary pressure scaling approach, particularly the assumption of a steady-state system, as discussed in previous research (16, 40).

In addition, a detailed statistical analysis of the 3D saturation profiles is presented in **Figure 6 c-h**, comparing the experimentally measured saturations with those simulated for the decane-brine and CO_2-brine scenarios at specific time points. The histograms (**Fig. 6 c,g**) show excellent agreement over a wide range of saturations, an agreement that is further supported by the correlation plots (**Fig. 6 d,h**), which show correlation coefficients above 0.99 and 0.98 for the decane and CO_2 scenarios, respectively. The discrepancies between experimental and simulated data occur mainly at higher brine saturation levels, indicating known experimental errors in the saturation measurements, but are not considered significant for the current study.

4. SUMMARY AND CONCLUSIONS

This study provides important insights into multiphase flow in heterogeneous rock formations with heterogeneities on the order of millimeters to tens of centimeters, which can be studied in laboratory experiments but must be averaged in reservoir simulations. The present study questions the direct applicability of relative permeability derived from special core analysis (SCAL) in such cases. This question is particularly relevant in view of the growing importance of carbon capture and storage as a countermeasure to climate change and its associated risks. Accurately predicting the migration of CO_2 plumes in underground reservoirs is crucial for assessing the risks associated with CO_2 storage and is the subject of the present study. The study was conducted with a very heterogeneous rock type and with CO_2-brine, a fluid pair that tends to amplify the effect of heterogeneity on two-phase fluid displacement. However, the developed numerical workflow can be extended to other highly heterogeneous/demanding rock-fluid systems.

In this paper, we first show that the direct application of SCAL data to describe CO_2-brine displacement on a larger experimental scale cannot be satisfactorily described if the rock is heterogeneous. This is to be expected, since the underlying assumption that the sample is representative and homogeneous in all rock properties is not justified, which must also apply to the description of two-phase flow in a grid block at the reservoir scale. However, history matching of the experimental data with a homogeneous model provides good agreement with the experimental responses. The resulting relative permeability can be considered upscaled and representative for the volume under study but differs significantly from the $k_r(S_w)$ derived from SCAL and may still be scale dependent. However, to be able to use standardized SCAL experiments, the heterogeneity of the rock must be taken into account in one way or another at the sub-grid scale.

The inclusion of the 1D porosity profile together with permeability and capillary scaling represents a first attempt to account for the effects of heterogeneity on two-phase flow. For this, we are applying a concept developed for steady-state experiments to USS experiments that are easier and faster to perform. The results show that the experimental data can be described quite well, especially the saturation profiles and the brine production curve for both systems, decane-brine and CO_2-brine. There are discrepancies in the transient behavior in the region of the breakthrough point, where the differential pressure is underestimated. A comparison of the resulting relative permeabilities for the decane-brine case shows that they are well within the uncertainty interval of the classical SCAL data. This suggests that SCAL data measured on homogeneous and small-scale samples do indeed provide a good description of two-phase displacements, provided that capillary heterogeneity is taken into account. The deviation of the obtained CO_2-brine relative permeabilities from the SCAL data indicates different wettabilities and interfacial tensions, since the SCAL data were measured with decane and brine as fluids.

An extension of the developed method to include heterogeneity in the two-phase modeling to a 3D grid for application to the 3D experimental domain shows comparable results. For this purpose, the calculated LED parameters of the best fit of the 1D heterogeneous simulation were used for the forward simulation in 3D. The exact statistics of the saturation distributions show a very good agreement between the 3D experimental and simulation data, which gives confidence in the developed methodology.

The main messages of this study are twofold:

a. An upscaled relative permeability can be perfectly derived from larger scale experiments using only the homogeneity assumption for numerical interpretation. This relative permeability may be different from a standard relative permeability and may still be scale dependent.
b. By introducing porosity-based heterogeneity and permeability and capillary scaling, standard relative permeability saturation functions well describe two-phase displacements even in a heterogeneous rock. However, the introduction of the explicit porosity map is more of a downscaling since it cannot be done at the reservoir scale.

To be able to use standard laboratory SCAL programs for CCS field development, (a) and (b) need to be bridged.

The authors propose to develop a method that upscales standard SCAL data, such as steady-state relative permeability ($k_r(S_w)$) and porosity maps from CT scans to a larger scale. However, there is a challenge: having a porosity map is not enough to capture all the heterogeneities in the rock; one would also need a water saturation map, as mentioned in **Equation 6**, to calculate the scaling factors (f). This requires a large core flooding experiment, which is beyond the scope of standard SCAL methods. However, by using X-rays to measure saturation changes during steady-state SCAL tests, it's possible to obtain both a gray-scale porosity map and a corresponding water saturation map from the same experiments. By carefully selecting rock samples that are very similar ("twin" samples) and using the steady-state $k_r(S_w)$ along with the porosity and water saturation (S_w) maps as inputs, it becomes possible to accurately predict flow in large-scale core floods using only the porosity information available.

In terms of finding "twin" samples and how many small samples are needed to accurately represent larger scale experiments, the strategy is inspired by a process described in Maas et al (30). Essentially, the process starts with one sample and checks whether its heterogeneity cut-off falls below a given threshold for heterogeneity. If it exceeds this threshold, then two samples are tested together, then three, and so on, until the combined variability of the samples is within acceptable limits. This step-by-step approach helps determine the right number of samples to use for accurate large-scale modeling, but without such detailed analysis, it's hard to give an exact number.

STATEMENTS AND DECLARATIONS

Author Contributions

Omidreza Amrollahinasab: Methodology, Investigation, Formal analysis, Writing – original draft. Boris Jammernegg: Investigation, Writing – review & editing. Siroos Azizmohammadi: Methodology, Writing – review & editing. Holger Ott: Conceptualization, Methodology, Supervision, Writing – original draft

Conflicts of Interest

There are no conflicts of interest to declare.

Data, Code & Protocol Availability

The code used to perform the analysis in this paper is open source at: https://github.com/omidreza-amrollahi/ad-scal-heterogeneous.

ORCID IDs

Omidreda Amrollahinasab https://orcid.org/0000-0002-6539-6304
Boris Jammernegg https://orcid.org/0009-0003-8653-6964
Siroos Azizmohammadi https://orcid.org/0000-0003-2258-111X
Holger Ott https://orcid.org/0000-0002-7297-9380

REFERENCES

1. Alpak, F. O., Zacharoudiou, I., Berg, S., Dietderich, J., & Saxena, N. (2019). Direct simulation of pore-scale two-phase visco-capillary flow on large digital rock images using a phase-field lattice Boltzmann method. *Computational Geosciences,* 23, 849–880. https://doi.org/10.1007/s10596-019-9818-0
2. Aminu, M. D., Nabavi, S. A., Rochelle, C. A., & Manovic, V. (2017). A review of developments in carbon dioxide storage. *Applied Energy,* 208, 1389–1419. https://doi.org/10.1016/j.apenergy.2017.09.015
3. Amrollahinasab, O., Azizmohammadi, S., & Ott, H. (2023). Simultaneous interpretation of SCAL data with different degrees of freedom and uncertainty analysis. *Computers and Geotechnics*, 105074. https://doi.org/10.1016/j.compgeo.2022.105074
4. Bear, J. (2013). *Dynamics of fluids in porous media*. Courier Corporation.
5. Berg, S., Oedai, S., & Ott, H. (2013). Displacement and mass transfer between saturated and unsaturated CO_2–brine systems in sandstone. *International Journal of Greenhouse Gas Control,* 12, 478–492. https://doi.org/10.1016/j.ijggc.2011.04.005
6. Berg, S., Unsal, E., & Dijk, H. (2021a). Non-uniqueness and uncertainty quantification of relative permeability measurements by inverse modelling. *Computers and Geotechnics,* 132, 103964. https://doi.org/10.1016/j.compgeo.2020.103964
7. Berg, S., Unsal, E., & Dijk, H. (2021b). Sensitivity and uncertainty analysis for parameterization of multiphase flow models. *Transport in Porous Media,* 140, 27–57. https://doi.org/10.1007/s11242-021-01576-4
8. Blunt, M. J. (1997). Pore level modeling of the effects of wettability. *SPE Journal, 2*(4), 494–510. https://doi.org/10.2118/38435-PAB
9. Brooks, R. H., Corey, A. T. (1964). Hydraulic properties of porous media and their relation to drainage design. Transactions of the ASAE, 7(1), 0026–0028. https://doi.org/10.13031/2013.40684
10. Burmester, G., Zekiri, F., Jurcic, H., Arnold, P., & Ott, H. (2022). Integration and Upscaling of Multi-Phase Fluid Flow Properties in Clastic Reservoirs. *83rd EAGE Annual Conference & Exhibition*, 1–5. https://doi.org/10.3997/2214-4609.202210939
11. Chang, J., & Yortsos, Y. C. (1992). Effect of Capillary Heterogeneity on Buckley-Leverett Displacement. *SPE Reservoir Engineering,* 7, 285–293. https://doi.org/10.2118/18798-PA
12. Egermann, P., & Lenormand, R. (2005). A new methodology to evaluate the impact of localized heterogeneity on petrophysical parameters (kr, Pc) applied to carbonate rocks. *Petrophysics,* 46. SPWLA-2005-v46n5a2
13. Georgiadis, A., Berg, S., Makurat, A., Maitland, G., & Ott, H. (2013). Pore-scale micro-computed-tomography imaging: Nonwetting-phase cluster-size distribution during drainage and imbibition. *Physical Review E,* 88, 033002. https://doi.org/10.1103/PhysRevE.88.033002
14. Georgiadis, A., Maitland, G., Trusler, J. P. M., & Bismarck, A. (2010). Interfacial tension measurements of the (H_2O + CO_2) system at elevated pressures and temperatures. *Journal of Chemical & Engineering Data,* 55(10), 4168–4175. https://doi.org/10.1021/je100198g
15. Hosseini, S. A., Lashgari, H., Choi, J. W., Nicot, J.-P., Lu, J., & Hovorka, S. D. (2013). Static and dynamic reservoir modeling for geological CO2 sequestration at Cranfield, Mississippi, U.S.A. *International Journal of Greenhouse Gas Control,* 18, 449–462. https://doi.org/10.1016/j.ijggc.2012.11.009
16. Hosseinzadeh Hejazi, S. A., Shah, S., & Pini, R. (2019). Dynamic measurements of drainage capillary pressure curves in carbonate rocks. *Chemical Engineering Science,* 200, 268–284. https://doi.org/10.1016/j.ces.2019.02.002
17. Jackson, S. J., Agada, S., Reynolds, C. A., & Krevor, S. (2018). Characterizing Drainage Multiphase Flow in Heterogeneous Sandstones. *Water Resources Research,* 54, 3139–3161. https://doi.org/10.1029/2017WR022282
18. Jackson, S. J., & Krevor, S. (2020). Small-Scale Capillary Heterogeneity Linked to Rapid Plume Migration During CO_2 Storage. *Geophysical Research Letters,* 47. https://doi.org/10.1029/2020GL088616
19. Kong, X., Delshad, M., & Wheeler, M. F. (2015). History matching heterogeneous coreflood of CO_2/brine by use of compositional reservoir simulator and geostatistical approach. *SPE Journal,* 20, 267–276. https://doi.org/10.2118/163625-PA

20. Krause, M., Krevor, S., & Benson, S. M. (2013). A procedure for the accurate determination of sub-core scale permeability distributions with error quantification. *Transport in Porous Media,* 98, 565–588. https://doi.org/10.1007/s11242-013-0161-y
21. Krause, M., Perrin, J.-C., & Benson, S. M. (2011). Modeling permeability distributions in a sandstone core for history matching coreflood experiments. *SPE Journal,* 16, 768–777. https://doi.org/10.2118/126340-PA
22. Krause, M. H., & Benson, S. M. (2015). Accurate determination of characteristic relative permeability curves. *Advances in Water Resources,* 83, 376–388. https://doi.org/10.1016/j.advwatres.2015.07.009
23. Kuo, C.-W., & Benson, S. M. (2015). Numerical and analytical study of effects of small scale heterogeneity on CO_2/brine multiphase flow system in horizontal corefloods. *Advances in Water Resources, 79*, 1–17. https://doi.org/10.1016/j.advwatres.2015.01.012
24. Kuo, C.-W., Perrin, J.-C., & Benson, S. M. (2011). Simulation studies of effect of flow rate and small scale heterogeneity on multiphase flow of CO_2 and brine. *Energy Procedia,* 4, 4516–4523. https://doi.org/10.1016/j.egypro.2011.02.408
25. Kurotori, T., & Pini, R. (2021). A general capillary equilibrium model to describe drainage experiments in heterogeneous laboratory rock cores. *Advances in Water Resources,* 152, 103938. https://doi.org/10.1016/j.advwatres.2021.103938
26. Leverett, M. C. (1941). Capillary behavior in porous solids. *Transactions of the AIME,* 142, 152–169. https://doi.org/10.2118/941152-G
27. Liu, Y., Gong, W., Zhao, Y., Jin, X., & Wang, M. (2022). A pore-throat segmentation method based on local hydraulic resistance equivalence for pore-network modeling. *Water Resources Research,* 58. https://doi.org/10.1029/2022WR033142
28. Lomeland, F., Ebeltoft, E., & Thomas, W. H. (2005). A new versatile relative permeability correlation. In *International Symposium of the Society of Core Analysts*, Toronto, Canada.
29. Lu, J., Kordi, M., Hovorka, S. D., Meckel, T. A., & Christopher, C. A. (2013). Reservoir characterization and complications for trapping mechanisms at Cranfield CO_2 injection site. *International Journal of Greenhouse Gas Control,* 18, 361–374. https://doi.org/10.1016/j.ijggc.2012.10.007
30. Maas, J. G., Springer, N., & Hebing, A. (2019). Defining a sample heterogeneity cut-off value to obtain representative Special Core Analysis (SCAL) measurements. In *International Symposium of the Society of Core Analysts*, Pau, France, 26–30 August.
31. McPhee, C., Reed, J., & Zubizarreta, I. (2015). *Core analysis: A best practice guide*. Elsevier.
32. Ni, H., Boon, M., Garing, C., & Benson, S. M. (2019). Predicting CO_2 residual trapping ability based on experimental petrophysical properties for different sandstone types. *International Journal of Greenhouse Gas Control,* 86, 158–176. https://doi.org/10.1016/j.ijggc.2019.04.024
33. Onoja, M. U., & Shariatipour, S. M. (2019). Assessing the impact of relative permeability and capillary heterogeneity on Darcy flow modelling of CO_2 storage in Utsira Formation. *Greenhouse Gases: Science and Technology,* 9, 1221–1246. https://doi.org/10.1002/ghg.1932
34. Øren, P.-E., Bakke, S., & Arntzen, O. J. (1998). Extending predictive capabilities to network models. *SPE Journal,* 3(4), 324–336. https://doi.org/10.2118/52052-PA
35. Ott, H. (2015). *CO_2-brine primary displacement in saline aquifers: Experiments, simulations and concepts* (Habilitationsschrift). RWTH Aachen.
36. Ott, H., de Kloe, K., van Bakel, M., Vos, F., van Pelt, A., Legerstee, P., Bauer, A., Eide, K., van der Linden, A., Berg, S., & Makurat, A. (2012). Core-flood experiment for transport of reactive fluids in rocks. *Review of Scientific Instruments,* 83, 084501. https://doi.org/10.1063/1.4746997
37. Ott, H., Pentland, C. H., & Oedai, S. (2015). CO2–brine displacement in heterogeneous carbonates. *International Journal of Greenhouse Gas Control, 33*, 135–144. https://doi.org/10.1016/j.ijggc.2014.12.004
38. Pini, R., & Benson, S. M. (2013a). Simultaneous determination of capillary pressure and relative permeability curves from core-flooding experiments with various fluid pairs. *Water Resources Research,* 49, 3516–3530. https://doi.org/10.1002/wrcr.20274
39. Pini, R., & Benson, S. M. (2013b). Characterization and scaling of mesoscale heterogeneities in sandstones. *Geophysical Research Letters,* 40, 3903–3908. https://doi.org/10.1002/grl.50756
40. Pini, R., Krevor, S. C. M., & Benson, S. M. (2012). Capillary pressure and heterogeneity for the CO_2/water system in sandstone rocks at reservoir conditions. *Advances in Water Resources,* 38, 48–59. https://doi.org/10.1016/j.advwatres.2011.12.007
41. Raoof, A., & Hassanizadeh, S. M. (2012). A new formulation for pore-network modeling of two-phase flow. *Water Resources Research,* 48. https://doi.org/10.1029/2010WR010180
42. Renard, P., & de Marsily, G. (1997). Calculating equivalent permeability: a review. *Advances in Water Resources,* 20, 253–278. https://doi.org/10.1016/S0309-1708(96)00050-4

43. Reynolds, C. A., Blunt, M. J., & Krevor, S. (2018). Multiphase flow characteristics of heterogeneous rocks from CO_2 storage reservoirs in the United Kingdom. *Water Resources Research, 54*, 729–745. https://doi.org/10.1002/2017WR021651
44. Reynolds, C. A., & Krevor, S. (2015). Characterizing flow behavior for gas injection: Relative permeability of CO_2-brine and N_2-water in heterogeneous rocks. *Water Resources Research, 51*, 9464–9489. https://doi.org/10.1002/2015WR018046
45. Ringrose, P. S., Sorbie, K. S., Corbett, P. W. M., & Jensen, J. L. (1993). Immiscible flow behaviour in laminated and cross-bedded sandstones. *Journal of Petroleum Science and Engineering,* 9, 103–124. https://doi.org/10.1016/0920-4105(93)90071-L
46. Ruspini, L. C., Øren, P. E., Berg, S., Masalmeh, S., Bultreys, T., et al. (2021). Multiscale digital rock analysis for complex rocks. *Transport in Porous Media,* 139, 301–325. https://doi.org/10.1007/s11242-021-01667-2
47. Valvatne, P. H., & Blunt, M. J. (2004). Predictive pore-scale modeling of two-phase flow in mixed wet media. *Water Resources Research,* 40. https://doi.org/10.1029/2003WR002627
48. Wellington, S. L., & Vinegar, H. J. (1987). X-ray computerized tomography. *Journal of Petroleum Technology,* 39(8). https://doi.org/10.2118/16983-PA
49. Wenck, N., Jackson, S. J., Manoorkar, S., Muggeridge, A., & Krevor, S. (2021). Simulating Core Floods in Heterogeneous Sandstone and Carbonate Rocks. *Water Resources Research,* 57. https://doi.org/10.1029/2021WR030581
50. Zhang, D., Zhang, R., Chen, S., & Soll, W. E. (2000). Pore scale study of flow in porous media: Scale dependency, REV, and statistical REV. *Geophysical Research Letters,* 27, 1195–1198. https://doi.org/10.1029/1999GL011101